JACS
JOURNAL OF THE AMERICAN CHEMICAL SOCIETY

ARTICLE

pubs.acs.org/JACS

Thixotropic Hydrogel Derived from a Product of an Organic Solid-State Synthesis: Properties and Densities of Metal−Organic Nanoparticles

Tamara D. Hamilton,[†] Dejan-Krešimir Bučar,[†] Jonas Baltrusaitis,[†,‡] Douglas R. Flanagan,[§] Yingjian Li,[§] Suman Ghorai,[†] Alexei V. Tivanski,*[,†] and Leonard R. MacGillivray*[,†]

[†]Department of Chemistry, 305 Chemistry Building, [‡]Central Microscopy Research Facility, 76 Eckstein Medical Research Building, and [§]Division of Pharmaceutics, College of Pharmacy, University of Iowa, Iowa City, Iowa 52242, United States

Supporting Information

ABSTRACT: Metallogels form from Cu(II) ions and tetratopic ligand *rctt*-1,2-bis(3-pyridyl)-3,4-bis(4-pyridyl)cyclobutane. The tetrapyridyl cyclobutane has been synthesized in the organic solid state. The gel forms with a variety of counteranions and gels water. The hydrogel is thixotropic and is composed of nanoscale metal−organic particles (NMOPs), a high surface area of which likely accounts for the gelation of the polar aqueous medium. A shear stress profile of the thixotropic hydrogel gave a yield value of 8.33 Pa. A novel combination of atomic force microscopy (AFM) and scanning transmission X-ray microscopy (STXM) is used to assess the densities of individual NMOPs. A density of 1.37 g/cm^3 has been determined. A single-crystal X-ray diffraction study demonstrates the ability of the unsymmetrical cyclobutane **3,4′-tpcb** to self-assemble with Cu(II) ions in $[Cu_2(hfac)_4(\mathbf{3,4'\text{-}tpcb})]_\infty$ (where hfac is hexafluoroacetylacetonate) to form a solvated 1D coordination polymer.

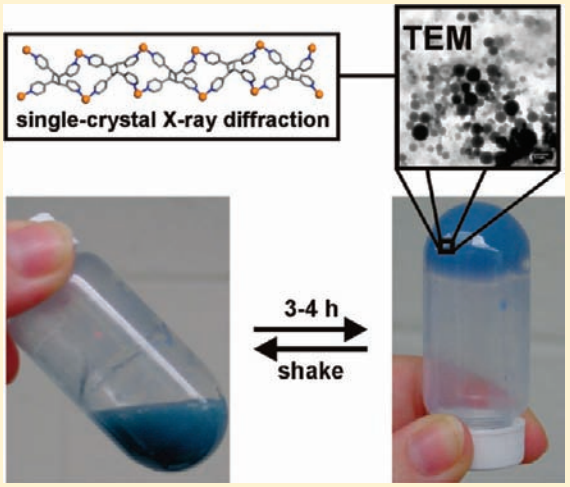

INTRODUCTION

The gelation of organic and aqueous solutions has applications in tissue engineering,[1] controlled drug release and delivery,[2−4] and pollutant sequestering.[5] Gelators are typically covalent polymers, however, gels sustained by molecular components that self-assemble via noncovalent forces (e.g., hydrogen bonding) are becoming more prevalent, particularly in the development of stimuli-responsive materials.[6−8] The process of gelation is considered to arise from the self-assembly of macromolecular components into networks that entangle and entrap solvent.[9] The formation of a gel represents a balance between the tendency of the components to dissolve and aggregate, which is especially important in the case of water as the solvent because the self-assembly process must compete with a dynamic network and the clustering of hydrogen bonds in the aqueous medium.[10]

In this context, metal−ligand bonding[11] has become an attractive means to gel organic and, to a lesser extent, aqueous solvents.[2,12−16] The incorporation of metals affords an opportunity to integrate the properties of metals (e.g., optical,[14,15] redox,[17] and magnetic[18]) into a supramolecular gel environment. An approach often used to form a metal−organic gel, or metallogel,[16] involves the self-assembly of metal ions with an organic ligand that bridges the metals in one, two, or three dimensions. The organic bridges are typically symmetric with respect to sites for metal ion coordination. To date, bridging ligands that support the formation of a metallogel have invariably been synthesized using conventional approaches to organic synthetic chemistry (i.e., solution-based methodologies).

In this report, we describe a metal−organic system that gels both organic and aqueous solvents[19,20] and is based on the ligand *rctt*-1,2-bis(3-pyridyl)-3,4-bis(4-pyridyl)cyclobutane (**3,4′-tpcb**) that has been synthesized in an unusual environment for a gel—the organic solid state (Scheme 1). We have described the template-directed solid-state synthesis[21] of **3,4′-tpcb** using 1,8-naphthalenedicarboxylic acid as a small-molecule hydrogen-bond-donor template.[22] The rigid, unsymmetrical tetratopic cyclobutane can bind up to four metal ions via the two different pyridine rings. Indeed, the ability of **3,4′-tpcb** to support a 2D metal−organic framework (MOF) composed of three different cavities that arise owing to the unsymmetrical nature of the ligand has very recently been reported.[23] The tetrapyridine is available from the solvent-free

Received: July 16, 2010
Published: February 22, 2011

dx.doi.org/10.1021/ja106095w | *J. Am. Chem. Soc.* 2011, 133, 3365–3371

Scheme 1. Solid-State Synthesis of 3,4′-tpcb and Metallogel Formation

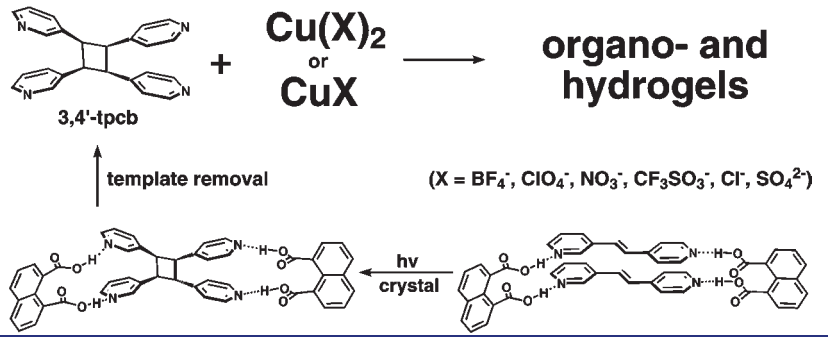

environment quantitatively, stereospecifically, and on a gram scale, which means that, in contrast to a majority of solid-state reactions, the cyclobutane is readily available for applications in coordination chemistry.

During studies aimed to construct crystalline MOFs with **3,4′-tpcb**,[21] we have discovered the ability of **3,4′-tpcb** to form gels with Cu(II) ions and a variety of counteranions in organic solvents and water. From transmission electron microscopy (TEM), the structure of the hydrogel is composed of recently discovered nanoscale metal−organic particles (NMOPs).[24−36] NMOPs are a class of inorganic−organic materials with promising applications in areas such as drug delivery,[34,35] molecular electronics,[27] biosensing,[32] and imaging.[36] To date, there have been no reports of NMOPs that support the formation of a gel, although colloidal metal−organic particles of micrometer dimensions have been reported.[24,28] Upon application of mechanical force, the hydrogel based on **3,4′-tpcb** turns liquidlike and thereby exhibits thixotropic behavior, which we have quantified by studying the shear stress response.[12,14,15,37−39]

From our studies involving **3,4-tpcb** as a building block of a gel, we also introduce here a method based on a combination of atomic force microscopy (AFM) and scanning transmission X-ray microscopy (STXM) to study the size-dependent densities of individual NMOPs. The densities of individual nanoparticles are, in general, difficult to determine. Whereas the densities of crystalline nanoparticles are assumed to be comparable to that of the bulk solid (e.g., Au = 19.3 g/cm^3),[40,41] the densities of amorphous particles can vary from the bulk owing to the presence of core particle inhomogeneities (e.g., voids).[41,42] An understanding of the properties of nanomaterials is critical for the fabrication of functional nanodevices. Differences in nanoparticle densities have been exploited, for example, in separation processes based on ultracentrifugation[40] whereas in biology, and the related field of medical diagnostics, correlations of densities of small biological particles with diseases are known yet measurement techniques can be laborious.[42] The combination of AFM and STXM described here uniquely offers a density quantification of nanoparticles on a single-particle basis and at the same time is quite practical. More specifically, we use AFM to determine the morphologies of individual NMOPs and STXM to measure C and N atomic absorbances that when combined provide a means to assess the densities of the particles. The NMOPs based on **3,4′-tpcb** reported here are shown to exhibit a density of approximately 1.37 g/cm^3, which is comparable to that of crystalline MOF materials.

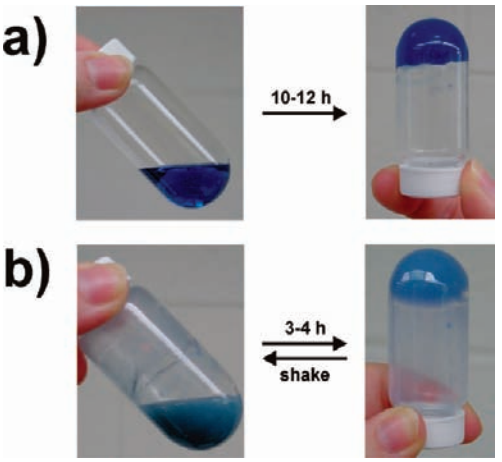

Figure 1. Metallogels upon combining $Cu(BF_4)_2 \cdot H_2O$ and **3,4′-tpcb**: (a) acetonitrile and (b) water.

RESULTS

Gel Formation from Organic Solvents. When **3,4′-tpcb** (0.0314 g, 0.086 mmol) was reacted with $Cu(BF_4)_2 \cdot H_2O$ (0.0210 g, 0.088 mmol, 1:1 ratio) in acetonitrile (4.0 mL), a blue solution immediately formed that after 10−12 h became a transparent blue gel (Figure 1). The experiment involving the organic solvent represents 2.0 wt % gelator, which is relatively low compared to that of most metallogels.[43] The blue color is consistent with each Cu(II) ion being coordinated by at least four pyridyl groups in an octahedral coordination geometry.[44] Gels also formed at gelator concentrations of between 1.0 and 2.0 wt % (Supporting Information). Thus, at 1.0 wt %, one gelator unit traps 1463 molecules of acetonitrile. Similar results were obtained using nitromethane as the solvent. A gel was not obtained, however, using either highly polar dimethylsulfoxide or dimethylformamide; instead, blue powders formed. Gels were obtained in methanol at higher weight percentages of gelator (ca. 10 wt %); however, below 2.0 wt %, solutions were obtained. Gels formed in acetonitrile and nitromethane using Cu(II) salts of ClO_4^-, NO_3^-, SO_4^{2-}, $SO_3CF_3^-$, and Cl^-. With Cu(II) hexfluoroacetylacetonate (hfac), a green crystalline powder was obtained.

The metallogels obtained from the organic solvents were thermally stable and did not display a change in morphology to well beyond the boiling points of each solvent. The level of stability has been reported only with gels based on purely organic

dx.doi.org/10.1021/ja106095w |J. Am. Chem. Soc. 2011, 133, 3365–3371

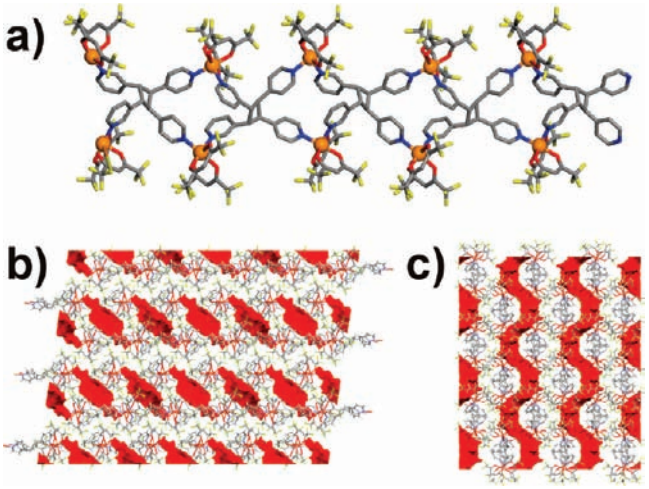

Figure 2. X-ray crystal structure of the 1D $[Cu_2(hfac)_4(\mathbf{3,4'\text{-}tpcb})]_\infty$: (a) crystallographic *a* axis, (b) crystal packing showing solvent inclusion along the *b* axis, and (c) packing showing solvent along the *c* axis. Solvent-occupied areas are in red (color scheme: C = gray, N = blue, O = red, F = yellow, and Cu = orange).

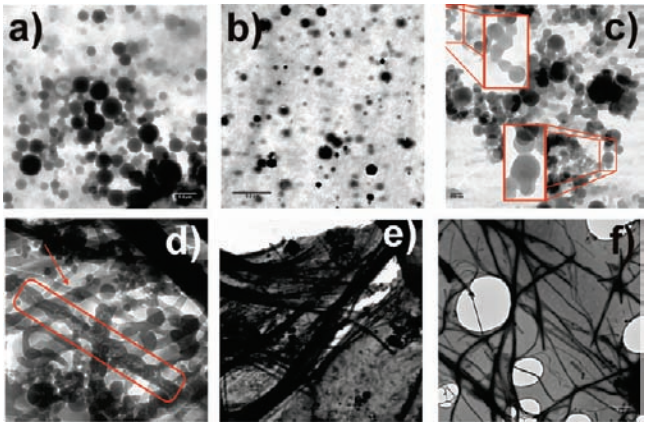

Figure 3. TEM micrographs of a hydrogel: (a) fresh gel upon standing (>4 h), (b) sol after shaking (5 min), (c) transition of NMOPs of reformed gel into "pearl-necklace" structures (in red) (3−6 weeks), (d) pearl-necklace nanostructures (red rectangle) and 1D nanobundles (red arrow) (6−12 weeks), (e) nanobundles and nanospheres (6−12 weeks), and (f) nanobundles in aged gels (about a year).

compounds.[45−47] When heated beyond the boiling point, the gels did not revert to a solution. Instead, a sticky, rubbery substance was present. The gels were also stable in capped vials on the benchtop without heating for more than 6 months.

X-ray Crystallography Analysis. To gain insight into the structures of the metallogels, single crystals from the reaction of **3,4′-tpcb** with $Cu(hfac)_2 \cdot H_2O$ were studied using X-ray diffraction. Thus, $[Cu_2(hfac)_4(\mathbf{3,4'\text{-}tpcb})]_\infty$ was prepared by layering a 10 mL acetonitrile solution of $Cu(hfac)_2 \cdot H_2O$ (0.034 g, 0.0685 mmol) on a 10 mL chloroform solution of **3,4′-tpcb** (0.025 g, 0.0685 mmol) (1:1 mol ratio). After a period of 1 day, green, rectangular single crystals of $[Cu_2(hfac)_4(\mathbf{3,4'\text{-}tpcb})]_\infty \cdot 1.6H_2O \cdot CH_3CN \cdot CHCl_3$ suitable for X-ray diffraction analysis formed at the solvent interface (yield: 0.037 g, 41%).

The components of $[Cu_2(hfac)_4(\mathbf{3,4'\text{-}tpcb})]$ assemble in the solid state to form a 1D coordination polymer[21] that is composed of rhomboids wherein **3,4′-tpcb** defines opposite corners of the polygons (Figure 2). The rhomboids have dimensions of ∼6.3 Å × 6.3 Å with corner angles of ∼80.2 and 110°. Each Cu(II) ion lies in an octahedral coordination environment and is coordinated by 4-pyridyl units and 3-pyridyl units in cis positions as well as two chelating $hfac^-$ anions. The separation distance between the metal centers is 7.87 Å within a polygon and 9.38 and 11.59 Å between adjoining polygons (Figure 2a). The cyclobutane ligand within each 1D polymer points in the same direction, or lies unidirectional, within each polymer strand as demonstrated by the orientations of the pyridyl groups. Neighboring strands pack antiparallel with included water, chloroform, and acetonitrile solvent molecules being disordered and filling the space between the strands (Figure 2b,c). The solvent present in the solid occupies approximately 16% of the unit cell. From the structure of $[Cu_2(hfac)_4(\mathbf{3,4'\text{-}tpcb})]_\infty$, we conclude that **3,4′-tpcb** lends itself to form infinite networks with Cu(II) ions. Infinite networks are considered to be the basic building units of gels.[23]

Gel Formation in Water. We have also discovered that the reaction of **3,4′-tpcb** (0.0485 g, 0.133 mmol) with $Cu(BF_4)_2 \cdot H_2O$ (0.0315 g, 0.133 mmol, 1:1 ratio) in water (4.0 mL) with minimum acetonitrile (<5%) results in a light-blue solution that after 3 to 4 h becomes a gel (Figure 1b). The experiment involving the water represents 2.0 wt % gelator. These observations make the metal−organic system a hydrogelator and a rare amphiphilic gelator. Gels also formed in water at concentrations of between 1.4 and 2.0 wt %. Thus, at 1.4 wt %, one gelator unit traps 2387 water molecules. Importantly, upon shaking, the hydrogel reverted to a sol that, upon standing for 3 to 4 h, reformed the gel. The transition between gel and sol was indefinitely repeatable. The ligand **3,4′-tpcb** thus supports the formation of a thixotropic hydrogel. Similar to the organogels, the hydrogel was thermally stable beyond the boiling point of the aqueous solvent. The hydrogel was also stable on a benchtop without heating or agitation for more than 6 months. When placed in a desiccator, the gel turned to a blue powder whereas re-exposure of the powder to water vapor resulted in the complete reformation of the gel.

TEM and AFM Studies of the Hydrogel. To obtain a picture of the aggregation mode of the hydrogel, samples at 2.0 wt % gelator were studied by TEM. A representative sample of a freshly prepared gel revealed spherical NMOPs of approximately 50−300 nm diameter (Figure 3a). The NMOPs were the primary particles visible in the TEM micrograph. A high-resolution TEM selected area electron diffraction (SAED) experiment[48] performed on several particles demonstrated the individual NMOPs to be amorphous. The particles compare in shape and size to recently reported NMOPs.[24,26,28,29,33,49] To our knowledge, the observation that NMOPs support the formation of a gel has not been described, although colloidal metal−organic particles of micrometer dimensions that support a gel have been reported.[24,28]

Representative images of the sol that immediately formed upon shaking (Figure 3b), as well as the reformed gel (Figure 3c), demonstrated that the NMOPs remained the primary particles within the sol and gel materials. Upon aging over periods of weeks, however, the spherical particles underwent a morphological transition into nanobundles and a 2D film (Figure 3d,e). The bundles appeared as pearl-necklace[50] structures from the fusion of the NMOPs. Similar transformations involving an organic charge-transfer dye[50] and a block copolymer have been described,[30] with

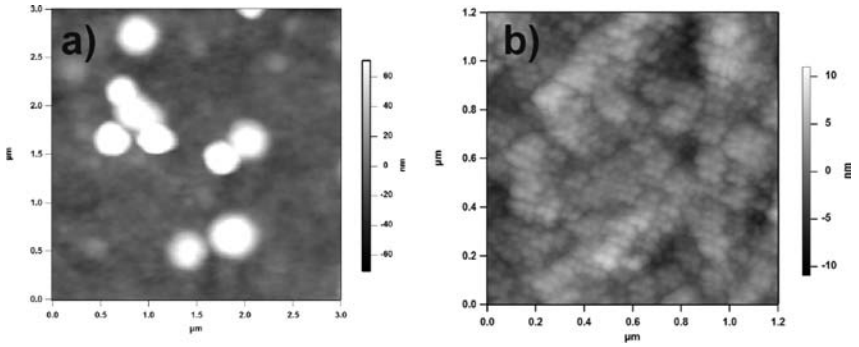

Figure 4. AFM height images showing the main particle morphologies of the hydrogel: (a) free nanoparticles with base sizes of approximately 300 nm and (b) nanoparticles within the films with typical heights of 4 to 5 nm and a base size of approximately 40 nm.

the origin of the transformations being attributed to the strain release of the high-curvature-energy contents of spherical particles and surface defects. For the system described here, the reversible nature of the metal−ligand bonding[24,49] in combination with the ability of the rigid tetrapyridine to enforce the components into 1D arrays likely accounts for the fusion of the NMOPs into thermodynamically more stable[50] bundles upon aging. The TEM micrographs also demonstrated that hydrogels were aged for up to 1 year to consist of aggregated and interwoven networks of nanobundles (Figure 3f).

To gain further insight into the morphology of the hydrogel, samples at 2.0 wt % gelator were studied using AFM (Figure 4). A representative AFM height image of a freshly prepared gel revealed the presence of NMOPs with base sizes of approximately 300 nm (Figure 4a), which were consistent with the TEM results. The heights, however, were several times smaller than the bases. In particular, an examination of 40 individual nanoparticles with sizes ranging between 50 and 900 nm revealed a height-to-diameter ratio of 0.36 ± 0.01. We attribute the deformation of the spheres to the release of included water via drying. A close inspection of the 2D film also revealed NMOPs with dimensions that were significantly smaller than those of the free nanoparticles (Figure 4b). The nanoparticles within the films exhibited heights of between 4 and 5 nm and bases of approximately 40 nm. With the films also being a major component of the gel, it is likely that the larger nanoparticles are able to transform to the smaller nanoparticles of the film.[24]

Thixotropy. To quantify the thixotropic behavior of the hydrogel, a series of shear stress loop tests were conducted. In particular, an extrapolation of the nearly linear portion of the increasing shear stress profile to the ordinate axis was determined to give a yield value of 8.33 Pa (Figure 5). The stress value is less than that for previously reported metallogels that gel organic solvents[37] and likely reflects difficulties of the NMOPs in maintaining strong surface contacts in the polar aqueous medium upon agitation. The low stress value can also be attributed to the relatively low concentration of the gelator (ca. 2%). Nevertheless, the ability of the components to form a gel in the highly polar aqueous medium is likely a result of the relatively small size of the NMOPs, which can provide a high surface area that supports many interparticle contacts and cross-links.[37] The formation of a large number of contacts and cross-links would also account for the high stabilities of the gels in the organic solvents.

Single-Particle Density from STXM and AFM. That the NMOPs exhibited approximately spherical morphologies prompted us to examine the densities of the nanoparticles using a combination

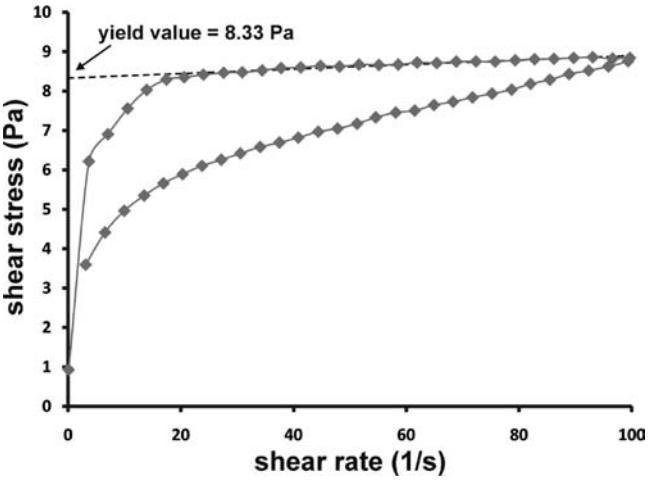

Figure 5. Shear stress vs shear rate graph for the 2% w/w thixotropic hydrogel based on $Cu(BF_4)_2$ and **3,4′-tpcb** showing a yield stress value of 8.33 Pa (indicated by an arrow). A stress ramp up and down producing shear rates from about 0 to 100 s^{-1} was used to elucidate the thixotropy of the hydrogel.

of synchrotron-based STXM and AFM.[51,52] STXM provides spatially resolved (~25 nm resolution) particle atomic absorbances (OD) that can quantified using Beer−Lambert's law[51]

$$\mathrm{OD}_i = \rho_i \mu_i h \qquad (1)$$

where i is the atom type (i.e., C, N, or O), OD_i is the total atomic absorbance in units of optical density (OD), μ_i is the mass absorption coefficient for the corresponding atom, ρ_i is the atomic density of the particle, and h is the particle height. Because STXM essentially measures the product of particle density and thickness, a density determination required a knowledge of the 3D shapes of the particles, which we obtained from the AFM results. Understanding the physical properties of individual nanoparticles (e.g., density) is important in the manipulation of nanoparticles and the fabrication of nanomaterials and devices. Moreover, by combining the AFM and STXM data, we expected to be able to determine the atomic density on a single-particle basis, according to eq 1. The combination of the methods could also, in principle, be extended to other nanoparticles and nanomaterials (e.g., aerosols).

In our STXM studies involving the NMOPs, single-energy (320 eV) STXM images of the particles (Figure 6a) were measured and determined to be consistent with the TEM and

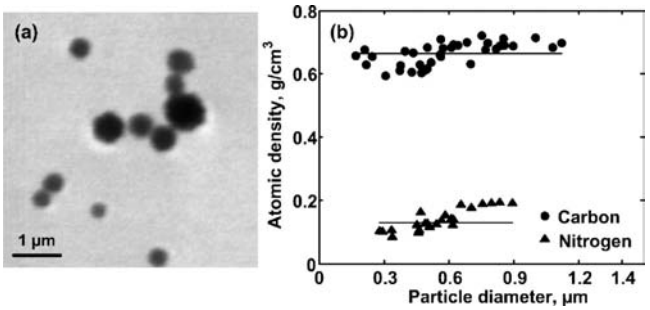

Figure 6. STXM data: (a) single-energy (320 eV, 5 μm × 5 μm) STXM image of NMOPs within the hydrogel and (b) single-particle C (•) and N (▲) atomic density vs particle diameter. Symbols are the data, and solid lines correspond to the averaged density.

AFM results. For a density quantification, absorbance maps for 36 and 25 individual NMOPs with size ranges of between 200 nm and 1.2 μm were collected at the C (320−280 eV) and N (420−395 eV) edges, respectively.[51] Oxygen absorbance maps (550−525 eV) were also collected for 15 individual NMOPs of various sizes; however, the maps displayed a complete absence of oxygen in the particles. We attribute the lack of O atoms to the NMOPs losing water and thus becoming fully dehydrated. However, both C and N maps indicated the presence of C and N atoms with uniform distributions throughout each particle (25 nm resolution), which is also indicative of uniform distributions of other atoms (H, Cu, B, and F) present in the particles. Total C and total N absorbances in OD units were next recorded at the center of each particle along with particle diameter. The height of each NMOP was determined by multiplying the diameter from STXM by 0.36, as determined from the AFM studies. The mass absorption coefficients were then calculated from the atomic scattering factors and determined to be 3.8 × 10^4 and 2.9 × 10^4 cm^2/g for C and N, respectively.[53] The single NMOP C and N atomic densities could then be determined by dividing the total C or N absorbance by the particle height and the corresponding mass absorption coefficient.

The single-particle C and N atomic densities were determined and plotted against particle diameter (Figure 6b). From the data, the mean values for the C and N densities were found to be 0.66 ± 0.04 and 0.13 ± 0.03 g/cm^3, respectively. The C/N ratio of atomic densities was thus calculated to be 5.14 ± 0.13. By scaling the C/N atomic density ratio with the atomic C and N weights, the ratio of the number of C to N atoms present in each NMOP was determined to be 6 ± 0.15. The resulting C/N ratio of approximately 6 was in excellent agreement with the molecular formula of **3,4′-tpcb**. By using a gel composition of [Cu(**3,4′-tpcb**)][$(BF_4)_2$][54] and assuming all atoms to be homogeneously distributed throughout each NMOP[42] as revealed by the STXM data, the atomic density was scaled to the total density of the nanoparticle. We calculated an average nanoparticle density of 1.37 ± 0.1 g/cm^3. The density is significantly smaller than that of the nanocrystals composed purely of metals (e.g., Au 19.3 g/cm^3)[41] yet is comparable to that of solvated crystalline MOFs and related metal−organic materials.[55−58] For the NMOPs described here, the density would likely correspond to that of a desolvated particle, which is consistent with the reduced height, or collapsed morphologies, of the individual particles. Metal-free nanoparticles such as polystyrene aerosols[59] (1.04 g/cm^3) and single-walled carbon nanotubes[40] (1.10 g/cm^3) generally exhibit smaller densities. To the best of our knowledge, the density of a NMOP has not been reported.

CONCLUSIONS

We have reported the ability of the multitopic ligand **3,4-tpcb** obtained from the organic solid state to support the formation of an amphiphilic metallogel. The hydrogel is thixotropic, which can be explained on the basis of the gel being composed of NMOPs that support many particle contacts. A novel combination of AFM and STXM has been used to determine the density of the NMOPs, with the density being comparable to that of MOF-based materials. The NMOPs have been determined to transform into bundles and films. We are currently employing additional ligands available from the organic solid state, and less available from solution, as the building blocks of metallogels. We are also focused upon determining whether the NMOPs can be developed for molecular encapsulation[26,33] with an aim toward expanding the ability of self-assembling gels to accommodate guest components trapped from aqueous media.

EXPERIMENTAL SECTION

Gel Materials. Solvents and reagents were purchased from Sigma-Aldrich Co. All chemicals were of reagent grade and were used without any further purification. **3,4-tpcb** was prepared according to the procedure described in a previous report.[22]

Syntheses of Gels. Solutions of **3,4′-tpcb** and an appropriate copper salt were combined in a 1:1 stoichiometric ratio at 2.0 wt % or less (combined) in various solvents (4.0 mL total). For the hydrogel, **3,4′-tpcb** was dissolved in a minimum amount (<0.150 mL) of anhydrous acetonitrile and combined with an aqueous solution of $Cu(BF_4)_2 \cdot H_2O$ in a 1:1 stoichiometric ratio at 2.0 wt % or less of gelator in doubly deionized water. The total volume of the resulting solution was brought to 4.00 mL. Gels were generally obtained after periods of 3 to 4 h.

X-ray Crystal Analysis of $[Cu_2(hfac)_4$(3,4′-tpcb)$]_\infty$. The diffraction data were measured on a Nonius Kappa CCD single-crystal X-ray diffractometer at low temperature using Mo Kα radiation (λ = 0.71073 Å). Data collection, cell refinement, and data reduction were performed using Collect[60] and HKL Scalepack/Denzo,[61] respectively. Structure solution and refinement were accomplished using SHELXS-97 and SHELXL-97,[62] respectively. A majority of non-hydrogen atom sites were identified upon structure solution using direct methods, whereas the remaining non-hydrogen atoms were indentified from the difference Fourier map within several refinement steps. All non-hydrogen atoms were refined anisotropically. Hydrogen atoms associated with carbon atoms were refined in geometrically constrained positions. Crystallographic data for $[Cu_2(hfac)_4$(**3,4′-tpcb**)$]_\infty$: $(C_{44}H_{24}Cu_2F_{24}N_4O_8) \cdot 1.6H_2O \cdot CH_3CN \cdot CHCl_3$, M_r = 1509.0 g mol^{-1}, monoclinic, $P2_1/c$ space group, a = 15.5534(16), b = 17.9540(18), c = 20.918(2) Å, β = 98.286(5)°, V = 5780.3(10) $Å^3$, Z = 4, ρ_{calc} = 1.73 g cm^{-3}, μ = 1.01 mm^{-1}, T = 190(1) K, $2\theta_{max}$ = 25.0°, a total of 24 831 collected reflections, 9166 unique reflections (R_{int} = 0.055), 6017 observed reflections [$I > 2\sigma(I)$], R_1(obs) = 0.092, wR_1(obs) = 0.251, R_2(all) = 0.125, wR_2(all) = 0.276, Δ_{rmax} = 0.970 e $Å^{-3}$, Δ_{rmin} = −0.56 e $Å^{-3}$, Mo Kα radiation (λ = 0.71070 Å). The structure contains highly disordered solvent molecules. The difference Fourier map revealed electron densities that could be ascribed to chloroform, acetonitrile, and water. Despite an extensive use of restraints, an acceptable solvent model was not achieved. The crystal structure was treated with the SQUEEZE routine of PLATON.[63] The solvent molecules were determined to occupy 899.5 $Å^3$ or 15.6% of the unit cell. An electron count of 385 electrons per unit cell corresponds to approximately 1 molecule of chloroform, 1 molecule of acetonitrile, and 1.6 molecules of water per asymmetric unit (CCDC-744648).

Rheology. Rheological measurements were performed with a Haake Rheostress 1 controlled stress rheometer operating with RheoWin (version 2.96) software with a cone and plate sensor (35 mm

diameter, 4° cone angle). To test a gel, approximately 1.2−1.3 g of gel was carefully applied to the lower plate and the cone sensor was lowered into position at a final rate of 0.3 mm/min; excess gel that emerged from the cone/plate was carefully wiped away from the edge so that only gel retained between the cone and plate remained. Once the cone reached its final position, the gel was allowed to relax for 3 min before a rheological test was initiated. The rheometer was used in a controlled rate mode with a range of shear rates from about 0 to 100 s^{-1}. The shear-stress ramp increased from low to high stress over about 1 min, and then the stress was decreased back to zero in about 1 min. The dwell time at each shear stress was 2 s. In a series of measurements, the gels exhibited nominally different separations between curves, with extrapolations of the nearly linear portions of the increasing shear-stress profiles to the ordinate axis giving yield values ranging from 8 to 12 Pa.

TEM Studies. The gel was placed on a carbon-coated copper grid, and the excess was removed with filter paper. The sample was then dried at reduced pressure and examined using a JEOL 1230 TEM at an 80.0 kV accelerating voltage. Images were acquired using a Gatan UltraScan 1000 2k × 2k CCD camera.

AFM Studies. The gel was placed on an atomically flat mica substrate or a Si_3N_4 window (Silson Ltd., England) and dried for at least 24 h under an ambient environment. The sample was examined using a commercial AFM (MFP 3D, Asylum Research, Santa Barbara, CA). AFM height image measurements were obtained at room temperature using silicon probes (Mikromasch, San Jose, CA, CSC37) with a typical tip radius of curvature of 10 nm. Topographic images were collected using intermittent contact mode (ac mode) at a typical scan rate of 1 Hz. All experiments were performed at room temperature under an ambient environment.

STXM Studies. The gel was placed on a Si_3N_4 window (Silson Ltd., England) and dried for at least 24 h in an ambient environment. Single-energy images and carbon, oxygen, and nitrogen K-edge NEXAFS spectra were acquired using an STXM instrument on beamline 5.3.2 of the Advanced Light Source (Berkeley, CA) in an ∼0.5 atm He-filled chamber. For these measurements, the X-ray beam is focused with a custom-made Fresnel zone plate onto the sample with a diffraction-limited spot size of 25 nm and the transmitted light intensity is detected. Images at a single energy are obtained by raster scanning the sample at the focal plane of X-rays and collecting transmitted monochromatic light as a function of the sample position. Spectra at each image pixel or a particular sample region are extracted from a collection of images recorded at multiple, closely spaced photon energies across the absorption edge. Dwell times used to acquire an image at a single photon energy were typically 1 ms per pixel. To quantify the absorbance signal, the measured transmitted intensity (I) is converted to optical density (OD) using Beer−Lambert's law: OD = $-\ln I/(I_0)$, where I_0 is the incident photon flux intensity. The incident beam intensity is measured through the sample-free region of the substrate. The particle spectrum is obtained by averaging over the particle deposited on the substrate. The X-ray energy calibration (accuracy of ±0.05 eV) is afforded by the addition of CO_2 gas (6 Torr) to the STXM chamber through a comparison of the position of CO_2 Rydberg transitions at 292.74 and 294.96 eV.[64]

NEXAFS spectra from 1s electrons for C, N, and O atoms were collected in the energy regions of 280−320, 395−420, and 525−550 eV, respectively. The pre-edge background typically arises from the weak but finite absorption of other elements at that energy. The postedge absorbance depends on the number of corresponding atoms at the particular edge (i.e., the number of carbon atoms at the C edge or oxygen atoms at the O edge). The total C, N, and O atomic absorbances were defined as the difference between the corresponding postedge and pre-edge absorbences. Pre-edge absorbences at 280, 395, and 525 eV and postedge absorbences at 320, 425, and 550 eV were used to quantify the total number of C, N, and O atoms.

■ ASSOCIATED CONTENT

Supporting Information. Synthesis procedures for the preparation of the gels. Supplementary crystallographic data can be obtained free of charge from the Cambridge Crystallographic Data Centre via www.ccdc.cam.ac.uk/conts/retrieving.html (CCDC 744648). This material is available free of charge via the Internet at http://pubs.acs.org.

■ AUTHOR INFORMATION

Corresponding Author
len-macgillivray@uiowa.edu; alexei-tivanski@uiowa.edu

■ ACKNOWLEDGMENT

We thank the National Science Foundation (L.R.M., DMR-0801329; J.B., AGS-0927944) for supporting this work. S.G. and A.V.T. gratefully acknowledge the University of Iowa for financial support. The work at the Advanced Light Source (ALS) of Lawrence Berkeley National Laboratory (LBNL) was supported by the Office of Science, Office of Basic Energy Sciences, the Division of Chemical Sciences, Geosciences, and Biosciences, and the Division of Materials Sciences of DOE at the ALS and LBNL under contract no. DE-AC03-76S00098. We thank A. D. Kilcoyne for support at beamline 5.3.2.

■ REFERENCES

(1) Lee, K. Y.; Mooney, D. J. *Chem. Rev.* **2001**, *101*, 1869–1880.
(2) Xing, B.; Choi, M.-F.; Xu, B. *Chem. Commun.* **2002**, 362–363.
(3) Tiller, J., C. *Angew. Chem., Int. Ed.* **2003**, *42*, 3072–3075.
(4) Li, J.; Ni, X.; Leong, K., W. *J. Biomed. Mater. Res. A* **2003**, *65A*, 196–202.
(5) Kiyonaka, S.; Sugiyasu, K.; Shinkai, S.; Hamachi, I. *J. Am. Chem. Soc.* **2002**, *124*, 10954–10955.
(6) Zhou, S.-L.; Matsumoto, S.; Tian, H.-D.; Yamane, H.; Ojida, A.; Kiyonaka, S.; Hamachi, I. *Chem.—Eur. J.* **2005**, *11*, 1130–1136.
(7) Estroff, L. A.; Addadi, L.; Weiner, S.; Hamilton, A. D. *Org. Biomol. Chem.* **2004**, *2*, 137–141.
(8) Bhuniya, S.; Park, S. M.; Kim, B. H. *Org. Lett.* **2005**, *7*, 1741–1744.
(9) Estroff, L. A.; Hamilton, A. D. *Chem. Rev.* **2004**, *104*, 1201–1218.
(10) Oshovsky, G. V.; Reinhoudt, D. N.; Verboom, W. *Angew. Chem., Int. Ed.* **2007**, *46*, 2366–2393.
(11) Swiegers, G. F.; Malefetse, T. J. *Chem. Rev.* **2000**, *100*, 3483–3538.
(12) Paulusse, J. M. J.; van Beek, D. J. M.; Sijbesma, R. P. *J. Am. Chem. Soc.* **2007**, *129*, 2392–2397.
(13) Fages, F. *Angew. Chem., Int. Ed.* **2006**, *45*, 1680–1682.
(14) Beck, J. B.; Rowan, S. J. *J. Am. Chem. Soc.* **2003**, *125*, 13922–13923.
(15) Weng, W.; Li, Z.; Jamieson, A. M.; Rowan, S. J. *Macromolecules* **2009**, *42*, 236–246.
(16) Piepenbrock, M.-O. M.; Lloyd, G. O.; Clarke, N.; Steed, J. W. *Chem. Rev.* **2009**, *110*, 1960–2004.
(17) Kawano, S.-I.; Fujita, N.; Shinkai, S. *J. Am. Chem. Soc.* **2004**, *126*, 8592–8593.
(18) Grondin, P.; Roubeau, O.; Castro, M.; Saadaoui, H.; Colin, A.; Clérac, R. *Langmuir* **2010**, *26*, 5184–5195.
(19) Miravet, J. F.; Escuder, B. *Chem. Commun.* **2005**, 5796–5798.
(20) Jung, J. H.; John, G.; Masuda, M.; Yoshida, K.; Shinkai, S.; Shimizu, T. *Langmuir* **2001**, *17*, 7229–7232.
(21) MacGillivray, L. R.; Papaefstathiou, G. S.; Friščić, T.; Hamilton, T. D.; Bučar, D.-K.; Chu, Q.; Varshney, D. B.; Georgiev, I. G. *Acc. Chem. Res.* **2008**, *41*, 280–291.

(22) Varshney, D. B.; Papaefstathiou, G. S.; MacGillivray, L. R. *Chem. Commun.* **2002**, 1964–1965.
(23) Hamilton, T. D.; Bučar, D.-K.; MacGillivray, L. R. *New J. Chem.* **2010**, *34*, 2400–2403.
(24) Oh, M.; Mirkin, C. A. *Nature* **2005**, *438*, 651–654.
(25) Johnson, C. A.; Sharma, S.; Subramaniam, B.; Borovik, A. S. *J. Am. Chem. Soc.* **2005**, *127*, 9698–9699.
(26) Champness, N. R. *Angew. Chem., Int. Ed.* **2009**, *48*, 2274–2275.
(27) Maeda, H.; Hasegawa, M.; Hashimoto, T.; Kakimoto, T.; Nishio, S.; Nakanishi, T. *J. Am. Chem. Soc.* **2006**, *128*, 10024–10025.
(28) Imaz, I.; Hernando, J.; Ruiz-Molina, D.; Maspoch, D. *Angew. Chem., Int. Ed.* **2009**, *48*, 2325–2329.
(29) Imaz, I.; Maspoch, D.; Rodríguez-Blanco, C.; Pérez-Falcón, J. M.; Campo, J.; Ruiz-Molina, D. *Angew. Chem., Int. Ed.* **2008**, *47*, 1857–1860.
(30) Vriezema, D. M.; Hoogboom, J.; Velonia, K.; Takazawa, K.; Christianen, P. C. M.; Maan, J. C.; Rowan, A. E.; Nolte, R. J. M. *Angew. Chem., Int. Ed.* **2003**, *42*, 772–776.
(31) Coronado, E.; Galán-Mascarós, J. R.; Monrabal-Capilla, M.; García-Martínez, J.; Pardo-Ibáñez, P. *Adv. Mater.* **2007**, *19*, 1359–1361.
(32) Rieter, W. J.; Taylor, K. M. L.; Lin, W. *J. Am. Chem. Soc.* **2007**, *129*, 9852–9853.
(33) Wenbin, L.; William, J. R.; Kathryn, M. L. T *Angew. Chem., Int. Ed.* **2009**, *48*, 650–658.
(34) Horcajada, P.; Chalati, T.; Serre, C.; Gillet, B.; Sebrie, C.; Baati, T.; Eubank, J. F.; Heurtaux, D.; Clayette, P.; Kreuz, C.; Chang, J.-S.; Hwang, Y. K.; Marsaud, V.; Bories, P.-N.; Cynober, L.; Gil, S.; Férey, G.; Couvreur, P.; Gref, R. *Nat. Mater.* **2010**, *9*, 172–178.
(35) Rieter, W. J.; Pott, K. M.; Taylor, K. M. L.; Lin, W. *J. Am. Chem. Soc.* **2008**, *130*, 11584–11585.
(36) Taylor, K. M. L.; Rieter, W. J.; Lin, W. *J. Am. Chem. Soc.* **2008**, *130*, 14358–14359.
(37) Weng, W.; Beck, J. B.; Jamieson, A. M.; Rowan, S. J. *J. Am. Chem. Soc.* **2006**, *128*, 11663–11672.
(38) Shirakawa, M.; Fujita, N.; Shinkai, S. *J. Am. Chem. Soc.* **2005**, *127*, 4164–4165.
(39) Lescanne, M.; Grondin, P.; d'Aleo, A.; Fages, F.; Pozzo, J. L.; Monval, O. M.; Reinheimer, P.; Colin, A. *Langmuir* **2004**, *20*, 3032–3041.
(40) Sun, X.; Tabakman, S., M.; Seo, W.-S.; Zhang, L.; Zhang, G.; Sherlock, S.; Bai, L.; Dai, H. *Angew. Chem., Int. Ed.* **2009**, *48*, 939–942.
(41) Sevonkaev, I.; Halaciuga, I.; Goia, D. V.; Matijević, E. *Colloids Surf., A* **2010**, *354*, 16–21.
(42) Godin, M.; Bryan, A. K.; Burg, T. P.; Babcock, K.; Manalis, S. R. *Appl. Phys. Lett.* **2007**, *91*, 123121–123123.
(43) The gelator weight is based on the combined weight of metal and organic components.
(44) Brown, D. H.; Nuttall, R. H.; McAvoy, J.; Sharp, D. W. A. *J. Chem. Soc. A* **1966**, *7*, 892–896.
(45) Snip, E.; Shinkai, S.; Reinhoudt, D. N. *Tetrahedron Lett.* **2001**, *42*, 2153–2156.
(46) Snip, E.; Koumoto, K.; Shinkai, S. *Tetrahedron* **2002**, *58*, 8863–8873.
(47) de Loos, M.; van Esch, J.; Stokroos, I.; Kellogg, R. M.; Feringa, B. L. *J. Am. Chem. Soc.* **1997**, *119*, 12675–12676.
(48) Mitran, E.; Dellinger, B.; McCarley, R. L. *Chem. Mater.* **2010**, *22*, 6555–6563.
(49) Sun, X.; Dong, S.; Wang, E. *J. Am. Chem. Soc.* **2005**, *127*, 13102–13103.
(50) Xu, J.; Liu, X.; Lv, J.; Zhu, M.; Huang, C.; Zhou, W.; Yin, X.; Liu, H.; Li, Y.; Ye, J. *Langmuir* **2008**, *24*, 4231–4237.
(51) Tivanski, A. V.; Hopkins, R. J.; Tyliszczak, T.; Gilles, M. K. *J. Phys. Chem. A* **2007**, *111*, 5448–5458.
(52) A comprehensive report outlining the applicability and limitations of the approach will be published elsewhere (Ghorai, S.; Alexandres, Z. J.; Tivanski, A. V., to be submitted for publication).
(53) Henke, B. L.; Lee, P.; Tanaka, T. J.; Shimabukuro, R. L.; Fujikawa, B. K. *At. Data Nucl. Data Tables* **1982**, *27*, 1–144.
(54) C and N K-edge NEXAFS spectra are consistent with all of the pyridine rings being coordinated with copper ions. (See Supporting Information.)
(55) Horike, S.; Shimomura, S.; Kitagawa, S. *Nat. Chem.* **2009**, *1*, 695–704.
(56) Phan, A.; Doonan, C. J.; Uribe-Romo, F. J.; Knobler, C. B.; O'Keeffe, M.; Yaghi, O. M. *Acc. Chem. Res.* **2009**, *43*, 58–67.
(57) Lee, J.; Farha, O. K.; Roberts, J.; Scheidt, K. A.; Nguyen, S. T.; Hupp, J. T. *Chem. Soc. Rev.* **2009**, *38*, 1450–1459.
(58) Kawano, M.; Fujita, M. *Coord. Chem. Rev.* **2007**, *251*, 2592–2605.
(59) Zelenyuk, A.; Cai, Y.; Chieffo, L.; Imre, D. *Aerosol Sci. Technol.* **2005**, *39*, 972–986.
(60) Hooft, R. W. W.; *COLLECT: Data Collection Software*; Nonius B. V., Ed.; Delft, The Netherlands, 1998.
(61) Otwinowski, Z.; Minor, W. *Methods Enzymol.* 1997, *276*, 307.
(62) Sheldrick, G. M. *Acta Crystallogr.* **2008**, *A64*, 112–122.
(63) Spek, A. L. *Acta Crystallogr.* **1990**, *A46*, C34.
(64) Ma, Y.; Chen, C. T.; Meigs, G.; Randall, K.; Sette, F. *Phys. Rev. A* **1991**, *44*, 1848.